



LUND UNIVERSITY

A Synthesis Method for Automatic Handling of Inter-patient Variability in Closed-loop Anesthesia

Soltesz, Kristian; van Heusden, Klaske; Hast, Martin; Ansermino, J. Mark; Dumont, Guy A.

Published in:
Proceedings of the 2016 American Control Conference

DOI:
[10.1109/ACC.2016.7526125](https://doi.org/10.1109/ACC.2016.7526125)

2016

Document Version:
Peer reviewed version (aka post-print)

[Link to publication](#)

Citation for published version (APA):
Soltesz, K., van Heusden, K., Hast, M., Ansermino, J. M., & Dumont, G. A. (2016). A Synthesis Method for Automatic Handling of Inter-patient Variability in Closed-loop Anesthesia. In *Proceedings of the 2016 American Control Conference* (pp. 4877-4882). IEEE - Institute of Electrical and Electronics Engineers Inc..
<https://doi.org/10.1109/ACC.2016.7526125>

Total number of authors:
5

General rights

Unless other specific re-use rights are stated the following general rights apply:
Copyright and moral rights for the publications made accessible in the public portal are retained by the authors and/or other copyright owners and it is a condition of accessing publications that users recognise and abide by the legal requirements associated with these rights.

- Users may download and print one copy of any publication from the public portal for the purpose of private study or research.
- You may not further distribute the material or use it for any profit-making activity or commercial gain
- You may freely distribute the URL identifying the publication in the public portal

Read more about Creative commons licenses: <https://creativecommons.org/licenses/>

Take down policy

If you believe that this document breaches copyright please contact us providing details, and we will remove access to the work immediately and investigate your claim.

LUND UNIVERSITY

PO Box 117
221 00 Lund
+46 46-222 00 00

A Synthesis Method for Automatic Handling of Inter-patient Variability in Closed-loop Anesthesia

Kristian Soltesz¹, Klaske van Heusden², Martin Hast¹, J. Mark Ansermino³, Guy A. Dumont²

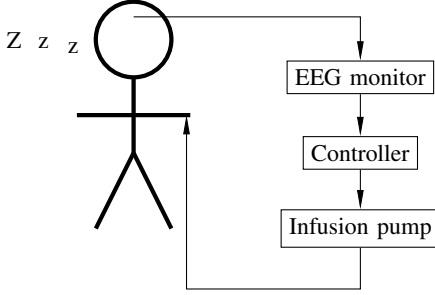


Fig. 1: Closed-loop anesthesia system.

Abstract—This paper presents a convex-optimization-based technique to obtain PID parameters, used to control the infusion rate of the anesthetic drug propofol. Controller design is based on a set of identified patient models, relating propofol infusion to an EEG-based consciousness index. The main contribution lies in the method automatically taking inter-patient variability into account, i.e., it guarantees robustness (sensitivity peak) and performance (disturbance rejection) over a set of patient models, without the need for manual intervention.

I. INTRODUCTION

This work considers closed-loop drug delivery in anesthesia. More specifically, propofol is dosed intravenously, to meet a desired consciousness level (also referred to as depth of hypnosis, DOH). The DOH is measured using the NeuroSense EEG monitor [1] and the hypnotic drug is administered by a computer-controller infusion pump. The control system is schematically depicted in Figure 1.

The main motivation for closed-loop controlled anesthesia is to reduce over-dosing, which could otherwise result in hemodynamic instability, and increases in both recovery time and post-operative mortality [2]. Clinical evaluation of several closed-loop systems has been reported [3], [4], [5], [6], [7], [8], [9]. These studies have shown the clinical feasibility of closed-loop anesthesia. However, for commercial products, it will be hard to demonstrate the safety of ad hoc control approaches. The main control challenge lies in robustly handling the large inter-patient variability in

the response to propofol [10]. In a simulation study [11], a model predictive control approach was suggested, for which robustness was evaluated in presence of limited inter-patient variability.

The authors have developed a PID controller based system that was successfully evaluated in a clinical study comprising 102 children [12]. Currently, it is being evaluated on adults in a study^a of 150 cases [13], and a second pediatric study is scheduled. In order to design safe closed-loop controllers, dynamic models of the patients' response to propofol are used, see Section II. As mentioned, such models hold large inter-patient variability, even after allometric regressions (such as scaling by patient weight). It is therefore critical that a closed-loop anesthesia delivery system be robust over the encountered inter-patient variability. For the study [12], this was achieved through robust loop shaping, evaluated over the set of available models [10], [14]. While providing robust controllers, the loop shaping was performed manually. Consequently, the controller design is suboptimal, and retuning of the controller is inefficient.

The novelty of this paper lies in the use of a recent convex-optimization-based synthesis method [15], removing the manual component from the synthesis procedure, while guaranteeing robustness up to a user-specified level. The method is demonstrated in two versions: one for producing a controller which performs robustly over a set of patient models, and one which performs robustly over an unstructured uncertainty description. The two versions of the synthesis method are demonstrated and compared, using models identified from clinical data [10]. A controller designed using the proposed method is scheduled for clinical evaluation.

II. PATIENT MODELS

A. PKPD Models

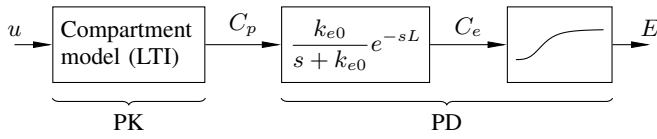
It is customary to model the patient's response to propofol using a pharmacokinetic (PK) model, dynamically relating infusion rate u to plasma concentration C_p , in series with a pharmacodynamic (PD) model, relating plasma concentration to clinical effect. The PK is traditionally modeled as a three-compartment mammillary model, i.e., a linear time invariant (LTI) system with three states. The PD model can be described by a first order time delay (FOTD) model, parametrized in k_{e0} , relating the plasma concentration C_p to the effect site concentration C_e , and a static sigmoid output nonlinearity, referred to as the Hill function. The latter can

¹Kristian Soltesz and Martin Hast are with the Department of Automatic Control, Lund University, Lund, Sweden. They are members of the LCCC and ELLIIT research centra. Correspondence: kristian@control.lth.se.

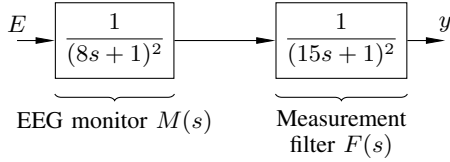
²Klaske van Heusden and Guy Dumont are with the Department of Electrical and Computer Engineering, University of British Columbia, Vancouver, Canada.

³J. Mark Ansermino is with the Department of Anesthesiology, Pharmacology and Therapeutics, University of British Columbia, Vancouver, Canada.

^aClinicalTrials.gov identifier: NCT01771263.



(a) PKPD patient model. The rightmost block represents the Hill function, defined through (1).



(b) EEG monitor and filter dynamics.

Fig. 2: Plant model, consisting of patient PKPD model, in series with EEG monitor and low-pass filter dynamics.

be written on the form

$$E(C_e) = \frac{E_0}{1 + (C_e/EC_{50})^\gamma}, \quad (1)$$

where C_e is the output of the LTI model, E is the clinical effect, and E_0 the clinical effect in absence of drug. In this paper E is scaled such that $0 \leq E_0 < 1$, while $E = 1$ corresponds to maximum clinical effect^b. EC_{50} is the solution to $E(EC_{50}) = (1 - E_0)/2$, i.e., the 50 % clinical effect, and γ is known as the "Hill parameter". A block diagram of the combined PKPD model is shown in Figure 2a.

PKPD models (i.e., LTI state space matrices, together with E_0 , EC_{50} , γ) for 47 children, identified from clinical data, were presented in [10] (together with corresponding low-order models, which could be used interchangeably, but would not be recognized by clinicians). Nyquist curves of the linearizations of these models (from u to E in Figure 2), around the (nominal clinical) operating point $E = EC_{50}$ are shown as thin lines in Figure 3. These LTI models are referred to as the *individual* models, and, for each angular frequency ω , form the set $P_{\text{all}} = \{P_1, \dots, P_n\}$ ^c.

The measurement of the clinical effect E is provided by means of the NeuroSense EEG monitor, which has LTI dynamics well approximated by $M(s) = 1/(8s + 1)^2$ [16]. A low-pass filter, $F(s) = 1/(15s + 1)^2$, is connected in series with the EEG monitor to reduce the effect of measurement noise. Without going into details, it should be mentioned that F must be chosen with the expected noise spectrum and open-loop high-frequency gain in consideration. Both M and F assume seconds as the unit of time. The relation between the clinical effect E and its measurement y , available for control, is shown in Figure 2b.

^bAn equivalent scaling where $E = 0$ and $E = 100$ corresponds to maximum and no clinical effect, respectively, is often found in the literature.

^cThe argument $i\omega$ will frequently be dropped to increase readability.

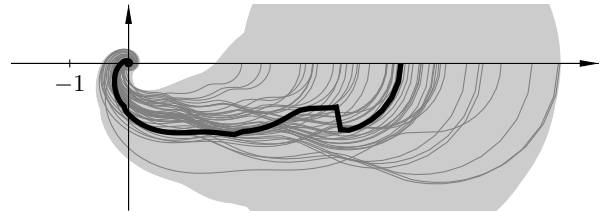


Fig. 3: Nyquist curve of linearized model from u to E , see Figure 2. Thin lines correspond to the individual models P . The thick black line is the nominal model P_0 , and the grey area represents the associated uncertain model $\tilde{P} = P_0 + \Delta$ (bottom and top, not crucial for robust design, truncated in figure).

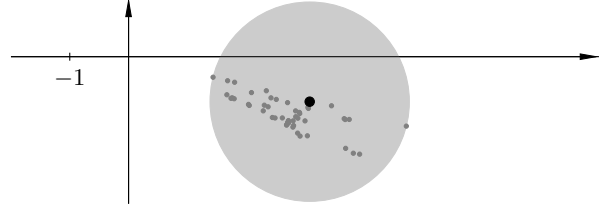


Fig. 4: Individual models (small marks), uncertainty region (grey disc) and nominal model (large mark) shown in the Nyquist plane. The figure is a subset of Figure 3, corresponding to a single frequency $\omega \in \Omega$.

B. Unstructured Uncertainty

An alternative to representing the inter-patient variability by a set of models, is to replace P with a nominal model P_0 and an additive uncertainty description Δ , forming the uncertain model $\tilde{P} = P_0 + \Delta$. To this end, a frequency grid $\Omega = \{\omega_1, \dots, \omega_m\}$ of sufficient span and density is chosen. In this paper a grid of $m = 1024$ logarithmically spaced frequencies, covering the phase range of interest for robust PID tuning is used. This grid is chosen so that $\max_P \angle FMP = -4.5\pi$ rad at ω_m .

The uncertain model \tilde{P} is defined at each $\omega \in \Omega$. A reasonable requirement is that P_0 lies in the convex hull of P and that Δ covers P , for each $\omega \in \Omega$. There are many ways to achieve this. Due to the safety critical nature of the application, and the synthesis method to be presented in Section III, a conservative formulation is chosen. The uncertainty Δ is defined, for each $\omega \in \Omega$, as the Nyquist-plane disc of smallest possible radius ρ , covering P , and P_0 as its center. This can be formulated, for each $\omega \in \Omega$, as

$$\begin{aligned} & \underset{P_0, \rho}{\text{minimize}} && \rho, \\ & \text{subject to} && |P - P_0| \leq \rho, \end{aligned} \quad (2)$$

which is a readily solvable convex program [17]. A graphical illustration, for the case $P = P_{\text{all}}$, is given in Figure 4. Figure 4 might give the impression that the uncertainty description is overly conservative, and that in fact most of the variability lies in model gain alone. However, this does not hold true for the range of frequencies (in the third Nyquist quadrant), which are critical for robust design. For these frequencies, the individual models (small marks) are more evenly spread over the uncertainty description (grey disc).

The nominal model P_0 and corresponding uncertainty discs Δ , for each $\omega \in \Omega$, are shown in Figure 3, as a thick black line and a grey area, respectively.

III. CONTROLLER SYNTHESIS

A. Optimization Problems

The existing, clinically evaluated [12], control system utilizes a PID controller^d $C(s) = k_p + k_i/s + k_d s$, with fixed measurement filter according to Figure 2b. When performing the loop shaping, performance was assessed through time-domain simulations of disturbance attenuation over the set of models, while robustness was maintained by limiting the maximum sensitivity magnitude over the model set.

In this paper, the same control structure as above, is assumed. The optimization objective is maximization of the integral gain k_i . This corresponds to minimizing the integral of the error (IE), caused by a load step disturbance [18]. Robustness is enforced by constraining the maximum sensitivity magnitude over Ω by M_s . This formulation enables the use of the synthesis method proposed in [15].

Two cases will be considered: one where optimization is performed over the model set P , and one where it is performed over the uncertain model \tilde{P} . These cases will be referred to as the *model set* and *uncertain-model* approach.

1) *Model Set Approach*: Let $K = FMC$ denote the series connection of controller, low-pass filter and EEG monitor dynamics, see Figure 2b. Optimizing over the set of models, the constraints are given by

$$\|S\|_\infty = \|1/(1 + P_k K)\|_\infty \leq M_s, \quad \forall P_k \in P. \quad (3)$$

The optimization problem can be formalized as

$$\begin{aligned} & \underset{k_p, k_i, k_d}{\text{maximize}} && k_i, \\ & \text{subject to} && 1/M_s - |L_k + 1| \leq 0, \\ & && \forall \omega \in \Omega, P_k \in P \end{aligned} \quad (4)$$

where $L_k = P_k K$ is the open-loop transfer function. The problem (4) has $\#(\Omega)\#(P)$ inequality constraints, where $\#$ denotes element count.

2) *Uncertain-Model Approach*: In the uncertain-model approach, as formulated in [15], (3) is slightly modified: S is exchanged for $\tilde{S} = 1/(1 + \tilde{P}K)$, eliminating the need to add individual constraints for each $P_k \in P$. The counterpart of (4) becomes

$$\begin{aligned} & \underset{k_p, k_i, k_d}{\text{maximize}} && k_i, \\ & \text{subject to} && 1/M_s + |K|\rho - |L_0 + 1| \leq 0, \\ & && \forall \omega \in \Omega \end{aligned} \quad (5)$$

where $L_0 = P_0 K$ is the nominal open-loop transfer. The number of inequality constraints is $\#(\Omega)$. This is a decrease by a factor $\#(P)$, compared with the model set approach.

^dThe ideal parallel form parametrization is used in favor of the more common standard form $C(s) = K(1 + 1/T_i s + T_d s)$, due to its linearity in the controller parameters.

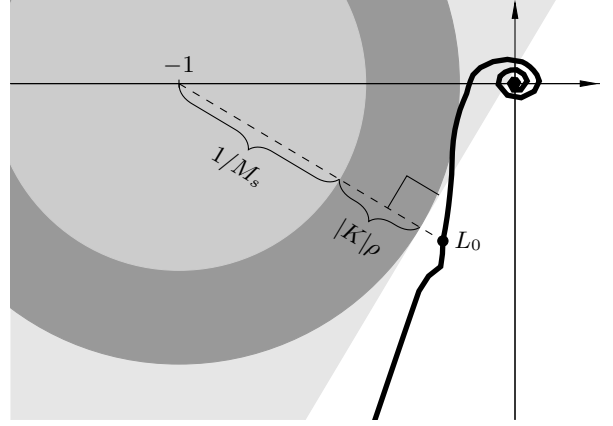


Fig. 5: Illustration of constraint linearization (for the uncertain-model case), used in the convex-concave procedure. The grey half plane corresponds to the convex relaxation through linearization. Note that the constraint shown in the figure is not active, since there is a distance between the half plane and L_0 .

B. The Convex-Concave Procedure

The constraints of both (4) and (5), correspond to circular disc in the Nyquist plane, which the open-loop transfer function(s) must avoid. In the model set approach, each open-loop Nyquist curve L_k must maintain a distance $1/M_s$ to -1 . In the uncertain-model approach, the nominal open-loop transfer function L_0 must maintain a distance $1/M_s + |K|\rho$ to -1 , where the second term is in place to ensure robustness over \tilde{P} , rather than only P_0 .

There is no efficient way to directly solve (4) or (5), as neither are convex programs (due to their constraints). A conservative approach, presented in [19], is to perform a convex relaxation. Each (non-convex) circle constraint is linearized, i.e., replaced by a half plane^e. This corresponds to exchanging $|L + 1|$, where $L = L_k$ in (4) and $L = L_0$ in (5) for

$$\Re \left(\frac{(L + 1)^*}{|L + 1|} (L + 1) \right), \quad (6)$$

where \Re denotes the real part and $*$ is the conjugate operator.

The convex relaxation honors constraints, since each circle is entirely contained in its corresponding half plane. However, the method is conservative for the same reason. This conservatism can be reduced by using the convex-concave procedure [20], which consists in iterating between performing the linearization (6) of (4) or (5) and solving the relaxed problem. (The solution of the last iteration is used to compute L for the next iteration.). It was demonstrated in [15] that the class of PID synthesis problems considered in this paper can be efficiently solved using the convex-concave procedure.

The procedure can be initialized with the zero controller $[k_p \ k_i \ k_d] = [0 \ 0 \ 0]$, since it fulfils the constraints for any asymptotically stable plant.

While there are no guarantees of reaching the true optimum, the convex-concave procedure monotonically increases

^eNote that each $\omega \in \Omega$ generates an individual half plane, see Figure 5.

the objective in its iterations, while honoring constraints. This makes it safe (in terms of robustness constraints), while the added iteration step makes it perform at least as well (in terms of objective) as a controller resulting from [19].

IV. DESIGN CASE STUDY

A. Background

The aforementioned control system has undergone a clinical trial on 102 children in the age group 6–17 years [12]. The controller tuning was slightly modified during this trial, based on the 47 patient models P_{all} , reported in [10], to arrive at the final PID parameter vector $[k_p \ k_i \ k_d] = [1.1 \ 0.0061 \ 66]$, see [14]^f. The above numeric values assume negative feedback in continuous time, u [$\mu\text{g/kg/min}$] (infused drug mass per patient weight per unit time), time scaled in seconds, and that E is scaled as described in Section II-A. (The actual control system is sampled at 5 s, but we will utilize continuous time to facilitate readability.)

A second scheduled trial comprises children with an (inclusive) upper age limit of 10 years. For this trial, a controller tuning, based on the subset P of the 47 available models, originating from children in the target age group, was requested. The new tuning was obtained using the proposed (automatic) method, in favor of (manual) loop shaping.

B. Controller Synthesis

Out of the 47 models in P_{all} , 20 were in the 6–10 (limits included) years age group. One outlier^g was removed, and the set P of the 19 remaining models was used for synthesis.

For the design example, we will ensure robustness by $M_s = 1.80$. For readers with a background in industrial control, this may seem like a large value. However, conservatism has been added at several stages along the design process:

- The patient models are inherently conservative, by purposeful over-estimation of their time delay [10].
- $M_s = 1.80$ corresponds to *worst case* (and not e.g. *mean*) robustness over the uncertain model \tilde{P} .
- The uncertainty model Δ was conservatively chosen, see Section IV-B.2 and Figure 6.

For the same model set, the maximum sensitivity modulus obtained with the previously evaluated controller was $M_s = 1.84$.

In all examples to follow, solving convex programs was done using CVX^h. Execution times refer to ones obtained using a normal desktop computer.

^fIn [14], controller parameters were reported in parallel form: $[K \ T_i \ T_d] = [-6.6m/100 \ 180 \ 60]$, assuming plant gain scaled by a factor $-1/100 \cdot 60 \text{ min/h}/(10 \text{ mg/ml}) \cdot m$, where m [kg] is the mass of the patient.

^gModel number 27 reported in [10] was removed. Occlusion of the propofol delivery line was registered during induction, and the resulting model had a very long estimated time delay.

^hCVX: a Matlab-based convex modeling framework, www.cvxr.com.

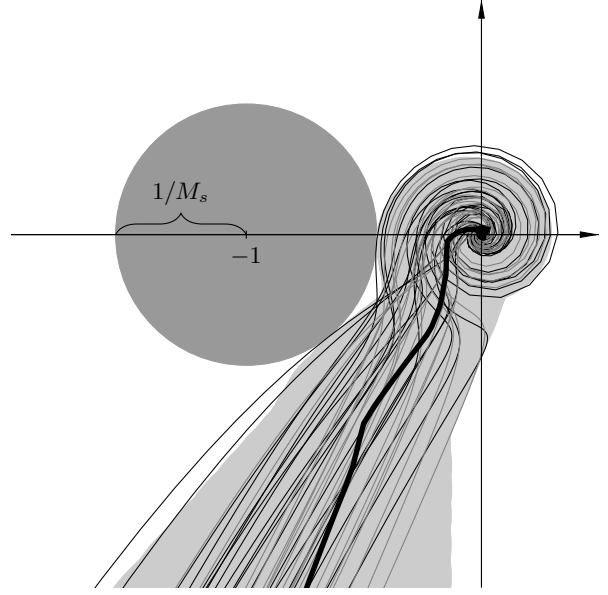


Fig. 6: Nyquist curve of the open-loop transfer with the resulting controllers. Model set approach: individual $L_k = P_k K_1$ (thin black), uncertain-model approach: nominal $L_0 = P_0 K_1$ (thick black), individual $L_k = P_k K_2$ (dark grey), and uncertain $\tilde{L} = \tilde{P} K_2$ (light grey). The dark grey disc needs to be avoided to fulfill the robustness constraint.

1) *Model Set Approach*: The solution of (4) took 19.5 s, and yielded the controller $K_1 = FMC_1$, where C_1 has parameter values $[k_p \ k_i \ k_d] = [1.4 \ 0.0074 \ 88]$. The corresponding open-loop Nyquist curves for $L_k = P_k K_1$ are shown as thin black lines in Figure 6. The distribution of $\|S\|_\infty$ over P is shown (light grey) in Figure 7.

2) *Uncertain-Model Approach*: The uncertain model \tilde{P} was computed from P , by solving $\#(\Omega) = 1024$ instances of (5). Each instance had $\#(P) = 19$ inequality constraints. The computation to obtain \tilde{P} took 58 s. The actual design, i.e. solving the convex relaxation of (5) with $\#(\Omega) = 1024$ inequality constraints took 3.4 s.

The resulting controller $K_2 = FMC_2$ has C_2 parametrized by $[k_p \ k_i \ k_d] = [1.3 \ 0.0056 \ 73]$. The resulting nominal open-loop Nyquist curve $L_0 = P_0 K_2$ (thick black), its uncertain counterpart $\tilde{L} = \tilde{P} K_2$ (light grey), and the individual open loops $L_k = P_k K_2$ (dark grey) are shown in Figure 6.

As indicated by Figure 6, the uncertainty characterization introduces conservatism. While the design was carried out with the constraint $M_s = 1.80$, the resulting worst case over P was $\|S\|_\infty = 1.68$ (with corresponding mean value $\|S\|_\infty = 1.34$). The distribution of $\|S\|_\infty$ over P is shown (dark grey) in Figure 7.

A Bode plot comparison between the final tuning used in the [12], [14] (dashed black) and the new designs K_1 (solid black) and K_2 (grey), is shown in Figure 8.

C. Simulation Results

The resulting controllers were evaluated on the 19 individual *nonlinear* models (see Section IV-B). Figure 9 shows how the controllers transition the simulated patients from their

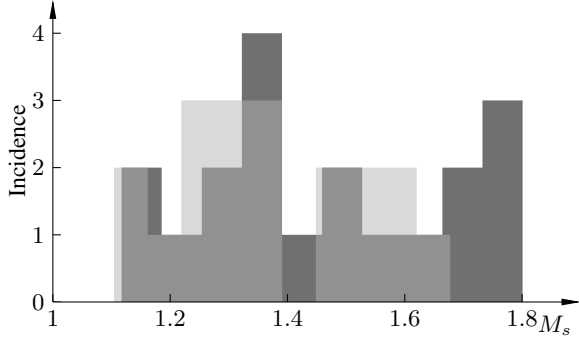
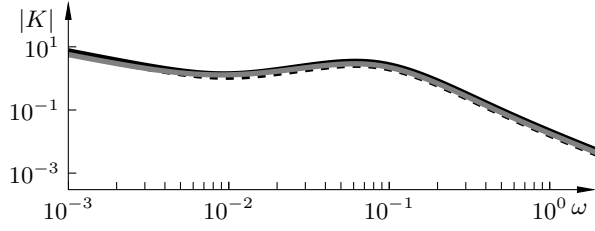
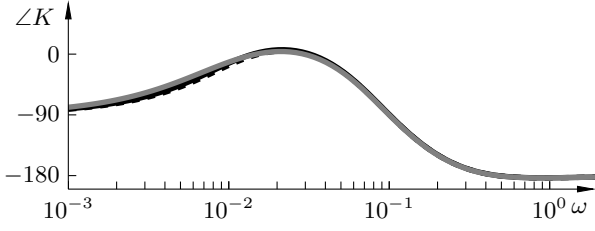


Fig. 7: Distribution of resulting $\|S\|_\infty$ over P for model set design K_1 (dark grey) and uncertain model design K_2 (light grey overlay).



(a) Magnitude.



(b) Phase (degrees).

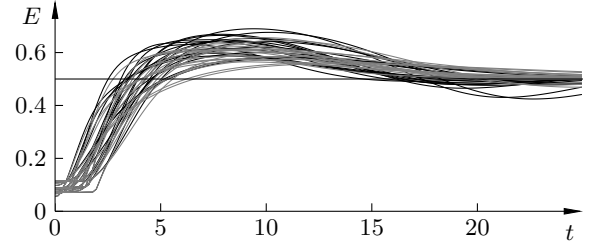
Fig. 8: Bode plots for K_1 (black) and K_2 (grey). The dashed black line correspond to the final tuning from [14]. (The unit for ω is rad/s.)

respective awake states $E = E_0$, to the setpoint $E = 0.5$. This transition is termed *induction* of anesthesia and the protocol (superimposed bolus) used for the simulations shown in Figure 9 is described in [12]. Black lines correspond to the model set design K_1 , grey lines correspond to the uncertain model design K_2 .

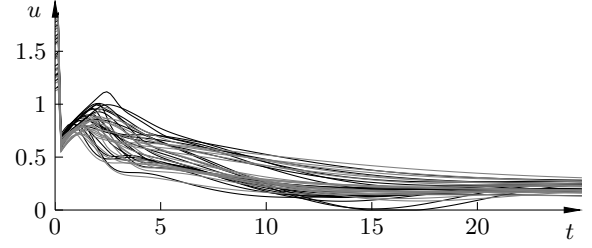
The *maintenance* phase begins upon induction of anesthesia. During this phase, it is the role of the controller to keep E steady, in the presence of disturbances. The most notable disturbance is caused by surgical stimulation. It decreases E , and is typically modeled as an additive output disturbance acting on the output of the PKPD model.

An output disturbance step of magnitude $\Delta E = -0.1$ was issued at $t = 0$ s, with simulations initiated at the equilibrium corresponding to $E = 0.5$. As is customary in many control contexts, we assume that the disturbance step response gives a fair assessment of the system's disturbance attenuation ability.

The outcome of these simulations are shown in Figure 10,



(a) Clinical effect. Black line shows setpoint.



(b) Drug infusion rate [$\mu\text{g/kg/min}$].

Fig. 9: Simulated induction of anesthesia, from $E = E_0$ to $E = 0.5$. Black and grey lines correspond to the model set and uncertain model designs K_1 and K_2 , respectively.

with line colors according to Figure 9. Although the control signals shown in Figure 9b and Figure 10b do not saturate, it is advisable to use an integrator anti-windup scheme in a clinical implementation, as was done in e.g. [14].

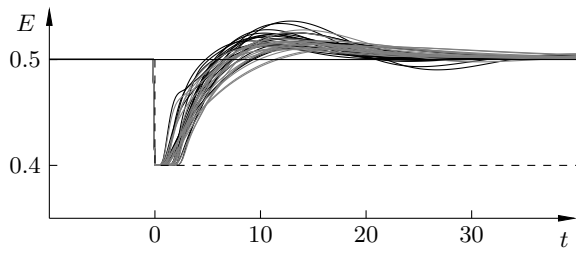
V. DISCUSSION

This paper proposes the use of the convex-concave procedure to obtain parameters for PID controllers, to be used in closed-loop controlled anesthesia. Feasibility has been demonstrated through a simulation case study, and a clinical trial of a controller obtained using the proposed method is currently scheduled.

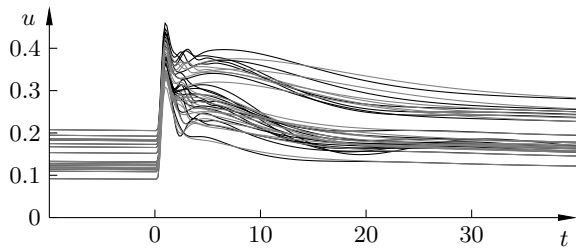
The proposed method has several advantages over the manual loop shaping strategy used previously in [14]. It is entirely automatic, honors user-specified robustness constraints and maximizes an objective directly linked to disturbance attenuation performance.

Two versions of the synthesis method were proposed: the model set approach of Section IV-B.1, and the uncertain model approach of Section IV-B.2. Key differences between these approaches are briefly discussed below.

The uncertain model approach, with unstructured uncertainty computes by solving (2), adds conservatism, as can be seen by comparing the thin black lines and light grey area in Figure 6. The amount of conservatism added at a specific frequency is determined by the spread in frequency response of the design model set P , as illustrated in Figure 4. A related aspect, seen in Figure 3, is that model uncertainty is large for small ω (near the steady state), but small throughout the phase range critical for robust design. This is a direct consequence of the experimental conditions under which data for identification of P was collected [10].



(a) Clinical effect. Horizontal black line shows setpoint. Black dashed line shows output disturbance profile.



(b) Drug infusion rate [$\mu\text{g/kg/min}$].

Fig. 10: Simulated disturbance rejection during maintenance of anesthesia. Black and grey lines correspond to the model set and uncertain model designs K_1 and K_2 , respectively.

We have seen that the computation of controller parameters is fast (time scale of seconds), while it is more expensive (time scale of minutes) to compute the uncertain model \tilde{P} . It can, however, be noted that \tilde{P} only needs to be computed once, upon which it can be used to solve several instances of the synthesis problem (to balance the trade-off between robustness and performance). Furthermore, the uncertain model approach results in constant time synthesis, regardless of the number of models used to generate the uncertain model \tilde{P} .

Which approach to choose depends on whether the extra conservatism introduced by the uncertain model \tilde{P} is desired, in combination with the number of elements of Ω and P . For the relatively small design example, with $\#(P) = 19$, presented in this paper, the time difference is not a critical design factor. However, scenarios where P consists of a large number of models, for which several designs are to be evaluated, would benefit from the uncertain model approach.

There is a close similarity between the controller presented in [14] and the herein proposed designs K_1 and K_2 . This similarity is seen both in the frequency response shown Figure 8 and in the simulation outcomes shown in Figure 9 and Figure 10. It indicates that the controller used in [12] is close to optimal, in the sense considered in this paper. It also indicates that the methods proposed in this paper can be used to obtain clinically feasible controllers.

Finally, it can be noted that the constraint level M_s can be used to shift the trade-off between robustness and performance. That is, faster disturbance attenuation is possible, but it comes at the cost of decreased robustness to inter-patient variability.

REFERENCES

- [1] T. Zikov, S. Bibian, D. G., H. M., and C. Ries, "Quantifying cortical activity during general anesthesia using wavelet analysis," *IEEE Trans. Biomed. Eng.*, vol. 53, no. 4, pp. 617–632, 2006.
- [2] J. Rinehart and C. Canales, "Closed-loop pharmacology in anesthesia and critical care: Benefits and limitations," *International Anesthesiology Clinics*, vol. 53, no. 3, pp. 91–101, 2015.
- [3] G. D. Puri, P. J. Mathew, I. Biswas, A. Dutta, J. Sood, S. Gombar, S. Palta, M. Tsering, P. L. Gautam, A. Jayant, M. D. Morup, *et al.*, "A multicenter evaluation of a closed-loop anesthesia delivery system: A randomized controlled trial," *Anesthesia and analgesia*, 2015.
- [4] N. Liu, T. Chazot, S. Hamada, A. Landai, N. Biochut, C. Dussaussoy, B. Trillat, L. Beyond, E. Samain, D. I. Sessler, and M. Dischler, "Closed-loop coadministration of propofol and remifentanyl guided by bispectral index: A randomized multicenter study," *Anesthesia & Analgesia*, vol. 112, no. 3, pp. 546–557, 2011.
- [5] N. Liu, T. Chazot, A. Genty, A. Landais, A. Restoux, K. McGee, P.-A. Laloë, B. Trillat, L. Barvais, and M. Fischler, "Titration of propofol for anesthetic induction and maintenance guided by the bispectral index: Closed-loop versus manual control: A prospective, randomized, multicenter study," *Anesthesiology*, vol. 104, no. 4, pp. 686–695, 2006.
- [6] Y. Sawaguchi, E. Furutani, G. Shirakami, M. Araki, and K. Fukuda, "A model-predictive hypnosis control system under total intravenous anesthesia," *Trans. Biomed. Eng.*, vol. 55, no. 3, pp. 874–887, 2008.
- [7] A. Gentilini, M. Rossoni-Gerosa, C. W. Frei, R. Wymann, M. Morari, A. M. Zbinden, and T. W. Schnider, "Modeling and closed-loop control of hypnosis by means of bispectral index (BIS) with isoflurane," *Trans. on Biomedical Engineering*, vol. 48, no. 8, pp. 874–889, 2001.
- [8] M. M. R. F. Struys, T. de Smet, F. Linda, M. Verschelen, S. van de Velde, R. van den Broecke, and E. P. Mortier, "Comparison of closed-loop controlled administration of propofol using bispectral index as the controlled variable versus standard practice controlled administration," *Anesthesiology*, vol. 95, no. 1, pp. 6–17, 2001.
- [9] M. Janda, O. Simanski, B. Pohl, G. F. Noeldge-Schomburg, and R. Hofmockel, "Clinical evaluation of a simultaneous closed-loop anaesthesia control system for depth of anaesthesia and neuromuscular blockade," *Anaesthesia*, vol. 66, no. 12, pp. 1112–1120, 2011.
- [10] K. van Heusden, J. M. Ansermino, K. Soltesz, S. Khosravi, N. West, and G. A. Dumont, "Quantification of the variability in response to propofol administration in children," *IEEE Trans. Biomed. Eng.*, vol. 60, no. 9, pp. 2521–2529, 2013.
- [11] R. Niño, J. abd de Keyser, S. Syafie, C. Ionescu, and M. Struys, "EPSAC-controlled anesthesia with online gain adaptation," *Int. J. Adapt. Control Signal Process.*, vol. 23, pp. 455–471, 2009.
- [12] N. West, G. A. Dumont, K. van Heusden, C. Petersen, S. Khosravi, K. Soltesz, A. Umedaly, E. Reimer, and J. M. Ansermino, "Robust closed-loop control of induction and maintenance of propofol anesthesia in children," *Pediatric Anesthesia*, vol. 23, no. 8, pp. 712–719, 2013.
- [13] S. M. Brodie, N. C. West, K. van Heusden, M. Görges, J. M. Andermino, G. A. Dumont, and R. N. Merchant, "Closed-loop controlled propofol anesthesia with remifentanyl administered either by target-controller infusion or closed-loop control," in *International Anesthesia Research Society Annual Meeting*, 2015, p. 120.
- [14] K. van Heusden, G. A. Dumont, K. Soltesz, C. L. Petersen, A. Umedaly, N. West, and J. M. Ansermino, "Design and clinical evaluation of robust PID control of propofol anesthesia in children," *IEEE Trans. Control Syst. Technol.*, vol. 22, no. 2, pp. 491–501, 2014.
- [15] M. Hast, K. J. Åström, B. Bernhardsson, and S. Boyd, "PID design by convex-concave optimization," in *Proc. European Control Conference*, IEEE, 2013, pp. 4460–4465.
- [16] S. Bibian, G. A. Dumont, and T. Zikov, "Dynamic behavior of BIS, M-entropy and neuroSENSE brain function monitors," *J. of Clinical Monitoring & Computing*, vol. 25, no. 1, pp. 81–87, 2010.
- [17] H. Hindi, C.-Y. Seong, and S. Boyd, "Computing optimal uncertainty models for frequency domain data," in *Proc. Conference on Decision and Control*, IEEE, 2002, pp. 2898–2905.
- [18] K. J. Åström, H. Panagopoulos, and T. Häggglund, "Design of PI controllers based on non-convex optimization," *Automatica*, vol. 34, no. 5, pp. 585–601, 1998.
- [19] M. Sadeghpour, V. de Oliveira, and A. Karimi, "A toolbox for robust PID controller tuning using convex optimization," in *Proc. Advances in PID Control*, IFAC, 2012, pp. 158–163.
- [20] A. L. Yuille and A. Rangarajan, "The convex-concave procedure," *Neural Computation*, vol. 15, no. 4, pp. 915–936, 2003.